



Synthesis and behavior of a magnetic composite based on crushed autoclaved aerated concrete for low-concentration phosphate removal

Weijie Li^{a,b,c,†}, Lixuan Zeng^{c,*,†}, Shu Lin^{a,b,*}, Fantang Zeng^{a,b}, Zhongya Fan^{a,b},
Zhiwei Huang^{a,b}

^aNational Key Laboratory of Water Environmental Simulation and Pollution Control, South China Institute of Environmental Sciences, Ministry of Environmental Protection, No. 18 Ruihe Road, Guangzhou 510535, China, Tel. +86 20 18902269938; email: linshu@scies.org (S. Lin), Tel. +86 20 13560004628; email: liweijie@scies.org (W. Li), emails: zengfantang@scies.org (F. Zeng), fanzhongya@scies.org (Z. Fan), huangzhiwei@scies.org (Z. Huang)

^bGuangdong Key Laboratory of Water and Air Pollution Control, South China Institute of Environmental Sciences, Ministry of Environmental Protection, No. 18 Ruihe Road, Guangzhou 510535, China

^cSchool of Chemistry and Environment, South China Normal University, 378 Waihuan West Road, Guangzhou 510006, China, Tel. +86 20 13640221972; email: zenglx@scnu.edu.cn

Received 3 July 2018; Accepted 12 November 2018

ABSTRACT

In this work, a novel magnetic composite using crushed autoclaved aerated concrete (MCAAC) as a carrier was prepared and applied to low-concentration (1 mg/L) phosphate removal. The structural and physical properties of MCAAC were characterized by X-ray fluorescence, X-ray diffraction, Fourier-transform infrared spectroscopy, scanning electron microscopy, energy-dispersive X-ray spectrometry, and saturation magnetization. Relevant mechanisms for phosphate removal under different conditions were also investigated. The adsorption and precipitation were studied separately to evaluate their roles in phosphate removal. The influence factors, including pH, calcium ion concentration, contact time, and Fe_3O_4 load, were studied and optimized. Results showed that MCAAC had been successfully synthesized and easily separated from the reaction mixture by a portable magnet. The phosphate removal rate by MCAAC reached 93.99% in the first 5 min and achieved reaction equilibrium (99.88%) in 120 min. The removal mechanism for low-concentration phosphate by MCAAC included a fast and large removal representing precipitation, then a slow and long removal due to adsorption. With the addition of phosphate, the pH and calcium ion concentration decreased in the suspension of MCAAC and hydroxyapatite ($\text{Ca}_5(\text{OH})(\text{PO}_4)_3$) formed on the surface of MCAAC, suggesting calcium phosphate precipitation may be a major mechanism in phosphate removal. Besides, comparison of the relative contribution of the adsorption and precipitation to the total removal of phosphate revealed that adsorption accounted for 20%–40%. The adsorption process was fitted to Langmuir model and pseudo-second-order kinetic model. All results demonstrated that MCAAC could be used as a promising material for low-concentration phosphate removal.

Keywords: Magnetic composite; Crushed autoclaved aerated concrete; Low-concentration phosphate; Removal mechanism

* Corresponding authors.

† These authors contributed the same amount of the work.

1. Introduction

Phosphate is often the limiting factor for primary production by phytoplankton in lakes. Due to widespread development of industry and agriculture in China, the release of excessive amounts of phosphate is responsible for the eutrophication of receiving waters, which results in the deterioration of water quality and overall ecological balance [1,2]. Hence, the removal of phosphate is paid more and more attention. To date, there have been various studies focusing on the removal of phosphate from the middle- and high-concentration solution [3–5]. However, as low as 0.2 mg/L phosphate into the surface water would stimulate the growth of aquatic micro and macro organisms and subsequently result in eutrophication [6,7]. Now phosphate at about 1 mg/L in the effluents from municipal sewage treatment plants can lead to eutrophication in relatively stagnant water bodies. So the removal of low-concentration phosphate should not be neglected. The commonly used methods to remove phosphate from wastewater include biological treatment [8], chemical precipitation [9,10], reverse osmosis [11], and adsorption [12–14]. Among these, adsorption and chemical precipitation are most widely accepted for low-concentration phosphate removal because of their high efficiency, low cost, and easy and simple operation. In this study, the methods of adsorption and chemical precipitation were employed to remove low-concentration phosphate from the aqueous solution.

In recent literatures, magnetic tetroxide iron (Fe_3O_4) had been widely applied to environmental remediation especially for phosphate removal [15–17]. The strong magnetic property of such particles enables solid–liquid separation using a simple magnet. Thus, effective composites coated with magnetic iron had been widely investigated to remove phosphate [18–20].

Crushed autoclaved aerated concrete (CAAC, Fig. 1), a kind of residues from building material, is made of simple or even waste ingredients (sand and fly ash) and mineral binders (lime and cement). Because CAAC is filled with oxides of aluminum, iron, and especially calcium which can strongly absorb and form precipitate with phosphate, the



Fig. 1. Crushed autoclaved aerated concrete (CAAC).

investigation on the reuse of CAAC should be drawn attention to. The studies of CAAC as an adsorbent and crystalline material to purify and recover the wastewater containing phosphate [21–24] had been investigated. Our previous study [25] had manifested that CAAC got high removal efficiency for low-concentration phosphate in alkaline condition ($\text{pH} > 10$) and obtained the better removal effect after modification by NaOH in neutral pH value. Nevertheless, CAAC as a lightweight material especially ground into powder could easily float on the water, which resulted in the difficulty of solid–liquid separation after treatment. Additionally, modification using NaOH would lead to secondary pollution caused by the waste alkaline solution.

To solve the abovementioned problems, magnetic crushed autoclaved aerated concrete (MCAAC), a novel material, coated with ferroferric oxide (Fe_3O_4) prepared by the coprecipitation of Fe^{3+} and Fe^{2+} with waste alkaline solution was presented in this study. The process of preparation included a neutralization step of the waste alkaline solution and addition of magnetism. The two steps not only prevented the generation of waste alkaline solution, but also attained a high efficiency and recovery for low-concentration phosphate removal. This paper describes the synthesis and properties of MCAAC, particularly in relation to the characteristics and removal mechanism for low-concentration phosphate.

2. Materials and methods

2.1. Materials

CAAC used in this experiment was obtained from a building material factory in Guangzhou, China, and ground to pass through a 100-mesh sieve. The main chemical compositions of CAAC obtained by X-ray fluorescence (XRF) are silicon, calcium, aluminum, iron, and small amount of other elements (Table 1). SiO_2 (48.11%) and CaO (28.59%) are the main constituents of CAAC.

2.2. Preparation of NCAAC

The CAAC modified by sodium hydroxide solution (NCAAC) was prepared under the following reaction conditions: reaction time 2 h, liquid/solid ratio 6 mL/g (150 mL/25 g), 2 M solution of NaOH, and temperature of 25°C. After being cooled down to room temperature, NCAAC was washed with doubly distilled water three times and twice with ethanol, then dried in an oven at 45°C, and ground to pass

Table 1
Chemical composition of CAAC

Compound (%)	CAAC
SiO_2	48.11
Al_2O_3	8.25
Fe_2O_3	5.39
CaO	28.59
MgO	0.74
K_2O	0.72
Na_2O	0.19
SO_3	0.67

through a 100-mesh sieve. The waste alkaline solution after centrifugation and modified products were stored in airtight containers for later experiments.

2.3. Preparation of Fe_3O_4

Fe_3O_4 was prepared through the coprecipitation of Fe^{3+} and Fe^{2+} . First, the solution of ferric chloride ($\text{FeCl}_3 \cdot 6\text{H}_2\text{O}$) and ferrous sulfate ($\text{FeSO}_4 \cdot 7\text{H}_2\text{O}$) with molar ratio of 4:3 was prepared and mixed together. Then the pH of the mixture was adjusted to 11 using waste alkaline solution. After being stirred at 60°C and crystallized at 70°C for 1.5 h, respectively, the mixture was separated with the aid of a permanent magnet and washed with deionized deoxygenated water several times till the pH value close to neutral. Finally Fe_3O_4 was prepared to magnet fluid of 50 wt% with deionized deoxygenated water, and then dried in a vacuum oven at 105°C and ground to pass through a 100-mesh sieve.

2.4. Preparation of MCAAC

The procedure for the synthesis of the MCAAC is illustrated in Fig. 2. Briefly, 1.5 g of ethyl carbamate and 5 mL 75% of ethanol were firstly mixed into a dilute binder in beaker. 1.5 g NCAAC and 0.5 g Fe_3O_4 was fully mixed in mortar then added in beaker for bonding. After being dried and ground in a similar manner to NCAAC, MCAAC was prepared.

2.5. Methods

Experiments were carried out by shaking 50 mL of 1 mg/L KH_2PO_4 (as P) solution at 200 rpm with 0.5 g of materials in the bottles capped with glass screws for 2 h (reaction time of 2 h was found to be enough for phosphate removal to achieve equilibrium in pre-experiments) at 25°C . The pH was adjusted to a given value by adding HCl or NaOH. After being shaken for 2 h, the suspensions were subsequently centrifuged, and the supernatants were determined for phosphate by the molybdenum blue ascorbic acid method. The Ca^{2+} concentrations were confirmed by calcium-Ethylenediamine tetraacetic acid titrimetric method. The pH in aqueous solution was

measured by using a pH meter with glass electrode. The residue after centrifugation was dried in an oven at 45°C and stored in airtight containers for later characterization. Deionized water, 1, 5, 10, 15, 20, 25, and 30 mg/L phosphate solution were used in the test, respectively, to conduct the following similar procedure, and the supernatants were used to determine pH and concentrations of Ca^{2+} ions. All experiments were conducted in duplicate, and the average values were used for data analysis.

All chemicals and reagents were used of analytical reagent grade. All glassware and sample bottles were soaked in diluted hydrochloric acid (HCl) solution for 12 h, washed, and then rinsed four times with deionized water. Deionized water was used for preparing all the solutions.

2.6. Characterization

The chemical compositions of CAAC were determined by energy-dispersive XRF (PW2404, PHILIPS Company). The X-ray diffraction (XRD) patterns were recorded using BRUKER D8 ADVANCE (Germany). Fourier-transform infrared spectroscopy (FT-IR) spectra were obtained by Nicolet 6700 (USA). The physicochemical properties of the materials were determined using scanning electron microscopy (SEM) (Zeiss Ultra 55, Germany), and energy-dispersive spectrometry (EDS) (Oxford X-Max 50, a manufacturer's product model of energy-dispersive spectrometry, was made by Germany) techniques. The hysteresis loops of samples are determined by vibrating sample magnetometer (VSM) which is made in Quantum Design, USA, and is MPMS (SQUID) XL-7 type.

3. Results and discussion

3.1. Characterization

The XRD patterns of the samples, including CAAC, NCAAC, pure magnetic Fe_3O_4 prepared with waste alkaline solution, and after phosphate removal, are investigated in Fig. 3. The main crystalline phases in CAAC are quartz (SiO_2 , 21.0° , 26.8° , 39.6° , 50.3° , 60.1°), tobermorite ($\text{Ca}_5\text{Si}_6\text{O}_{16}(\text{OH})_2 \cdot 4\text{H}_2\text{O}$, 29.1° , 29.6°), gypsum (CaSO_4 , 25.6°) and limestone (CaCO_3 , 38.8°). The characteristic

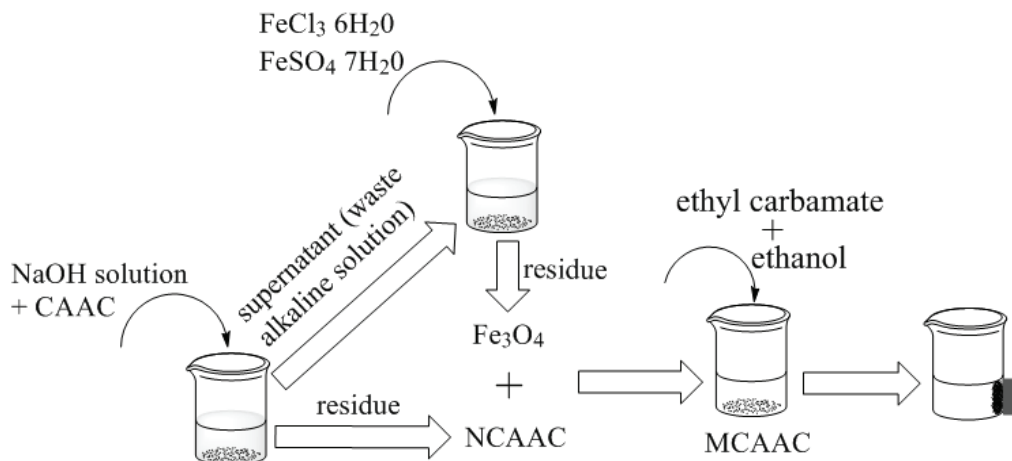
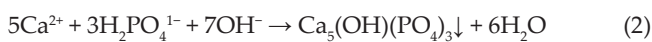
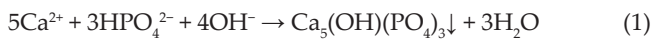


Fig. 2. The synthetic route of MCAAC.

diffraction peaks appeared in pure Fe_3O_4 at 30.2° , 35.1° , 43.5° , 54.1° , 57.4° , 63.1° could be assigned to [220], [311], [400], [422], [511], and [440] planes of magnetite (JCPDS card NO. 19-0629), respectively. The XRD pattern of MCAAC maintained the characteristic diffraction peaks of CAAC. The diffraction line at 2θ angle of 30.20° and 35.05° in MCAAC corresponded to magnetite [26,27], which indicated that Fe_3O_4 had been successfully gained and attached to the CAAC. Therefore, the synthesized MCAAC included the property of CAAC and magnetism. Meanwhile, the proportion of Fe_3O_4 in MCAAC only accounted for 25% theoretically, and, therefore, characteristic peaks of Fe_3O_4 were weak and broadened [28]. Comparison of MCAAC before and after phosphate removal showed the appearance of two sharp and intense peak characteristics of hydroxyapatite (HAP, $2\theta = 31.4^\circ$ and 31.9°) [3,29,30]. This result was similar to our previous study [25], which suggested that the main removal mechanism of phosphate by MCAAC is also according to the following equation:



Indeed, calcium phosphate compounds such as tricalcium phosphate ($\text{Ca}_3(\text{PO}_4)_2$) and calcium hydrogen phosphate (CaHPO_4) should be formed under alkaline condition. However, they are not observed in the XRD pattern. One reason is that due to their higher soluble phase than HAP, they will transform to HAP even if they are formed [3]. Another is possibly that they form amorphous insoluble precipitates which are not detected by XRD. Besides, the iron phosphate compounds are also not appeared in XRD, possibly due to that the content of iron in samples is not high enough to combine well with phosphate groups to form crystal. Additionally, the reflections of limestone, gypsum, and tobermorite are partly reduced or even absent after reaction, which explains that the ordered structure of them is partially

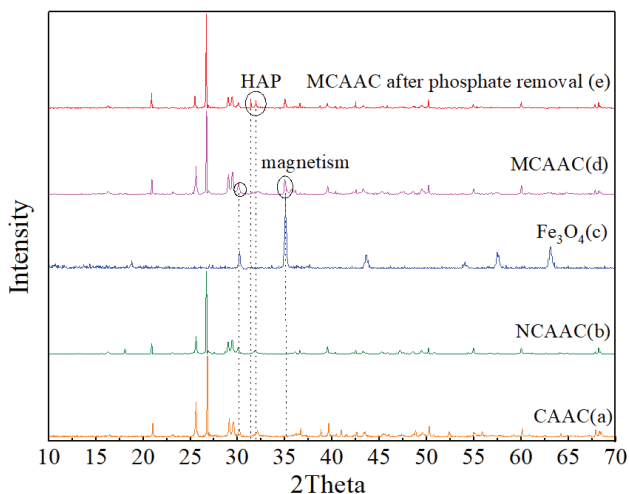


Fig. 3. X-ray diffraction patterns of (a) CAAC, (b) NCAAC, (c) pure Fe_3O_4 , (d) MCAAC, and (e) MCAAC after phosphate removal.

destroyed. Because of that, the Ca^{2+} can be released from MCAAC to solution and the insoluble substances (such as CaCO_3 and $\text{Ca}_5\text{Si}_6\text{O}_{16}(\text{OH})_2 \cdot 4\text{H}_2\text{O}$) in MCAAC will transform to HAP due to its lower solubility. According to the analyses, phosphate can be recovered by two aspects. On one hand, HAP once formed will not be easily released in a short time due to its low solubility, which increases the phosphate recovery in reaction. On the other hand, the samples with magnetism maintain the phosphate recovery after reaction.

The FT-IR spectra of samples including CAAC, NCAAC, and MCAAC are displayed in Fig. 4. These samples belong to hydrated material, and water adsorption bands at $1,616\text{ cm}^{-1}$, $1,660\text{ cm}^{-1}$, and in the range of $3,000\text{--}3,600\text{ cm}^{-1}$ indicated it. The bands at 464 cm^{-1} and 973 cm^{-1} were assigned to TiO_4 doable ring, and T–O bending, respectively (T = Si and Al). Another band observed at 674 cm^{-1} was due to Si–O–Ca bond. The CO_3^- band was detected at around $1,448\text{ cm}^{-1}$. A new characteristic peak related to Fe–O–Fe band of iron oxide appeared at 580 cm^{-1} [26], which indicated that Fe_3O_4 had been successfully attached on CAAC and supports the XRD analysis. In addition, the FT-IR spectra of MCAAC after phosphate removal exhibited new peak at $1,100\text{ cm}^{-1}$ (corresponding to the PO_4^{3-} vibration), which corresponded to the characteristic bands of HAP observed in XRD. Similarly, the presence of iron and other calcium phosphate compounds was not distinctly observed in the FT-IR spectra corresponding to the XRD analysis.

The SEM micrographs of CAAC, NCAAC, and MCAAC before and after phosphate removal are shown in Fig. 5. Fig. 5(a) shows the magnified SEM micrograph of CAAC included a large amount of irregular sheet particles mostly composed of calcium–silicate–hydrate. These irregular particles might be hollow particles filled with smaller pieces which were linked with the inner part of the particles. After modified by NaOH, the surface of NCAAC in Fig. 5(b) was coated with some pieces of crystalline materials whose sizes became more uniform compared with Fig. 5(a), possibly because of NaOH dissolving SiO_2 on the surface of CAAC. Fig. 5(c) reveals that the surface of MCAAC grew a number of uneven particles and became aggregative and rough compared with Fig. 5(b), which could be conjectured that

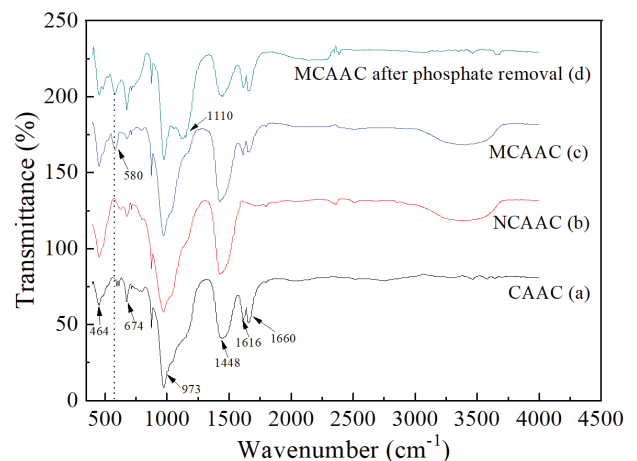


Fig. 4. FT-IR spectra of (a) CAAC, (b) NCAAC, (c) MCAAC, and (d) MCAAC after phosphate removal.

Fe₃O₄ attached to the surface of NCAAC. After phosphate removal, the surface of MCAAC in Fig. 5(d) looks like a tightly wrapped sphere.

EDS mapping analysis (Fig. 6) is performed to determine the chemical composition of the crystalline materials adhered to the surface of MCAAC. The EDS mapping analysis depicted in selected area (Fig. 5(d)) shows that the crystal on the surface of MCAAC appeared the elements of Ca and P, which supported the XRD and FT-IR analyses. In addition, other types of elements such as iron (Fe) and aluminum (Al) were also detected in EDS mapping analysis, which may explain that these metal ions were the component element of MCAAC or formed as amorphous insoluble precipitate on the surface of MCAAC. The presence of silicon (Si) was probably due to the dissolution of silicates in the MCAAC. The appearance of carbon (C) and oxygen (O) might be attributed to co-crystallization of calcium carbonate due to the carbonate alkalinity, and the reaction equation is as follows:

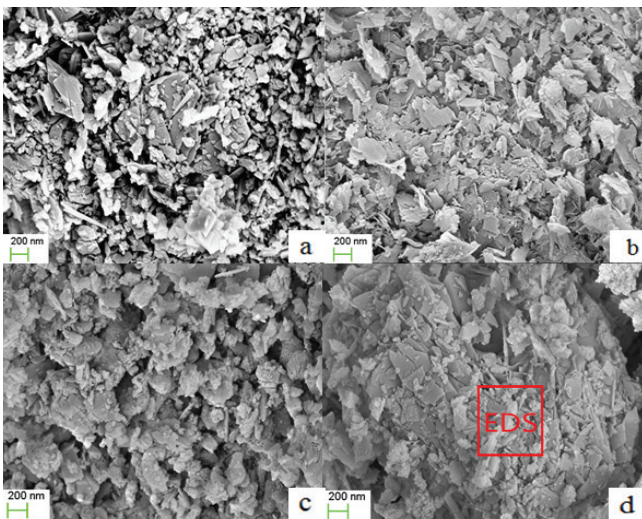
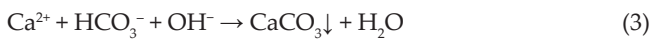


Fig. 5. SEM micrographs of (a) CAAC, (b) NCAAC, (c) MCAAC, and (d) MCAAC after phosphate removal.

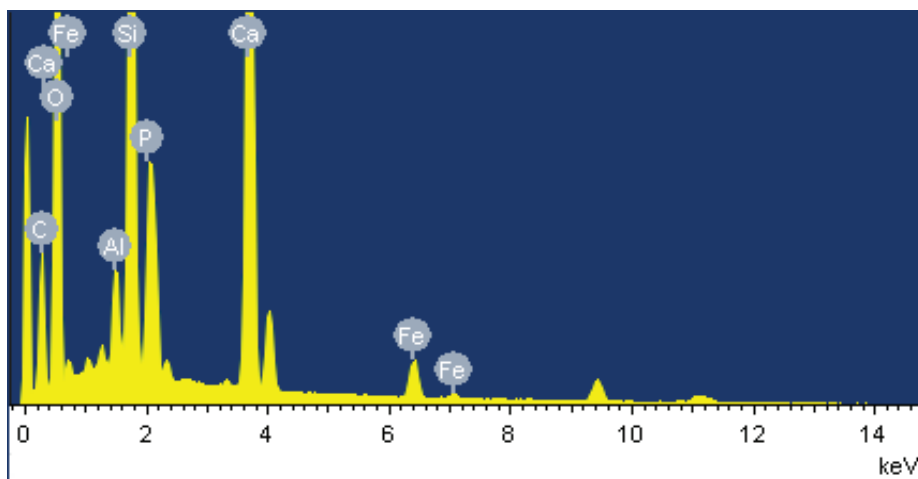


Fig. 6. EDS mapping analysis graph of MCAAC after phosphate removal.

The magnetization measurement determined with VSM (Fig. 7) displays that the saturation magnetization of MCAAC is about 0.6 emu/g. The magnetic curve showed no remanence and coercivity, which indicated that MCAAC had good super-paramagnetic property [31]. This value ensured that MCAAC had sufficient magnetic property to be attracted by a permanent magnet [32]. The separation ability of the MCAAC by an external magnet is demonstrated in Fig. 7. When a magnet was placed at one side of the bottle, homogeneously mixed MCAAC magnetic powder in bottle had been completely collected to the side close to magnet. Furthermore, the MCAAC could be separated from the solution with the help of an external magnet. This vivid phenomenon not only clearly confirms that MCAAC magnetic powder can be easily recovered by an external magnet but also verifies the results of characterization.

3.2. Effect of different Fe₃O₄ loading

The content of iron in MCAAC is an important parameter to test the recovery of phosphate and material. At the same time of adding magnetism to material, the variation of

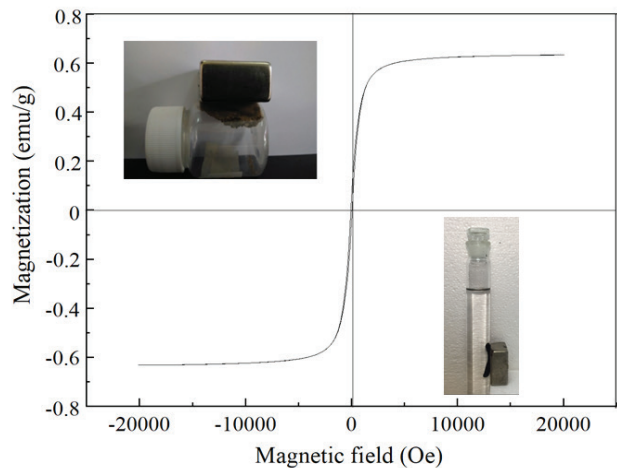


Fig. 7. Magnetization curve of MCAAC.

phosphate removal should be noticed. Fig. 8 reveals that the optimum content of iron in MCAAC accounts for 25% of total mass, which was corresponding the removal rate of 99.24%. However, the removal rate showed the tendency of decline when the content of iron exceeded 25% and reached the minimum at the content of 40% (93.19%). It was because that the increase of iron content would cover the surface of CAAC to block mutual contact area, which could influence the crystallization of HAP and individual adsorption.

3.3. Development of pH

The development of pH in MCAAC suspension with time is shown in Fig. 9. At the first 5 min, the pH of MCAAC after reaction in deionized water was 8.71, but with an addition of 1 and 5 mg/L of phosphate, the pH values decreased immediately to 7.21 and 7.13, respectively. Then, the pH values gradually increased with contact time and reached a peak value at 2 h. The final pH value of the MCAAC after reaction in deionized water was 10.18, while samples treated with a solution containing 1 and 5 mg/L phosphate had final pH values of

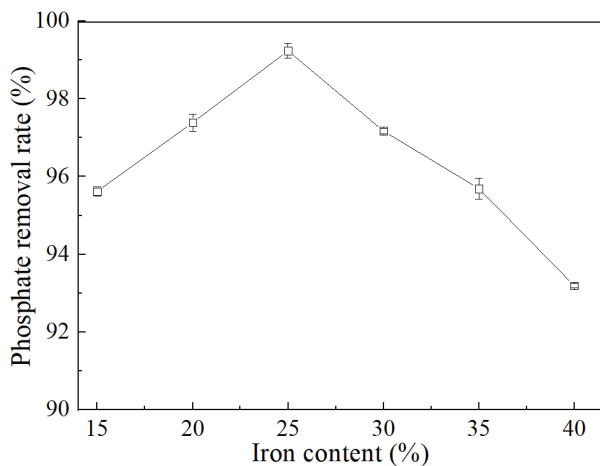


Fig. 8. Effect of Fe_3O_4 loading on phosphate removal.

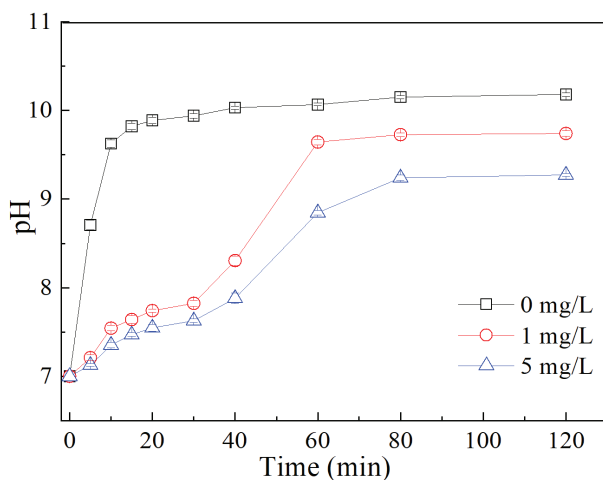


Fig. 9. Development of pH in MCAAC suspension with deionized water and 1 and 5 mg/L of phosphate solutions.

9.74 and 9.27, respectively. The high pH value of MCAAC in deionized water was due to dissolution of Ca^{2+} from the sample into the solution. When phosphate was reacted with the MCAAC, a large amount of Ca^{2+} was removed from the solution, resulting in the precipitation of calcium phosphate. The formation of calcium phosphate suppressed the change of pH.

3.4. Changes in calcium concentration and pH due to phosphate removal

It is suggested that phosphate removal depends on the dissolution of calcium ions (Ca^{2+}) from MCAAC. In order to find out the relationship between pH and dissolution of Ca^{2+} from MCAAC, a series of batch tests were performed. The results are presented in Fig. 10. The Ca^{2+} concentration and pH in MCAAC suspension was decreased with the addition of phosphate. Phosphate removal was accompanied by a reduction in the Ca^{2+} ion concentration and pH value, corresponding to the formation of HAP according to the characterizations. Phosphate may be removed by adsorption, but the results were not consistent with adsorption, a most important phosphate retention mechanism. With adsorption, it was difficult to explain the concomitant decrease of Ca^{2+} concentration that occurred as a result of phosphate addition. It was expected that the MCAAC containing large amounts of calcium and iron would adsorb phosphate and promote the precipitation of calcium and iron phosphates [10]. The concentration of phosphate declined more rapidly due to its direct precipitation with calcium.

3.5. Mechanism of low-concentration phosphat removal by MCAAC

Adsorption is another significant mechanism for phosphate removal. In order to compare the relative contribution of adsorption and precipitation to phosphate removal, the phosphate removal experiments of acidic (pH = 2) and neutral (pH = 7) conditions are presented in Table 2 and Fig. 11. At the acidic conditions, the initial and final pH values before and after reaction were adjusted and kept steadily

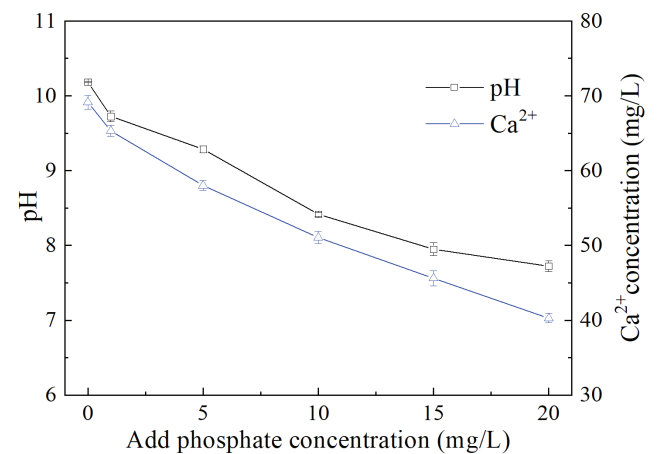


Fig. 10. The pH and Ca^{2+} concentration as a function for the amount of phosphate added.

at about 2. The removal of phosphate by MCAAC, CAAC, and Fe₃O₄ were investigated to the contribution of adsorption processes of phosphate. The samples treated with a solution containing 1 mg/L phosphate at the pH of 2 had final removal rate of 71.99%, 39.12%, and 19.16% for Fe₃O₄, MCAAC, and CAAC, respectively. It was obvious that phosphate removal by MCAAC had visibly improved compared with CAAC without modification, which suggested that the addition of Fe₃O₄ partly contributed to phosphate removal. At the pH of 7, phosphate removal by MCAAC in aqueous solution increased rapidly and reached 93.99% within 5 min due to its direct precipitation with calcium but considerably reduced (20.11%) compared with that the pH of 2. This was because that though insoluble calcium compounds or iron oxide in MCAAC would be dissolved to release calcium and iron ion under acidic condition, the phosphate groups (H₃PO₄) in aqueous solution hardly bonded with Ca²⁺ and Fe³⁺/Fe²⁺ to form precipitates. It could be considered that physical adsorption of MCAAC played a dominating role in acidic conditions instead of precipitation. The phosphate removal using MCAAC greatly increased in the pH range of 7–10.26, where the HPO₄²⁻ and PO₄³⁻ were the primary phosphate groups, and the high pH could cause PO₄-P to precipitate quantitatively as calcium and iron phosphates. Additionally, CaHPO₄ and Ca₃(PO₄)₂ would transform into HAP due to their lower solubility. The results indicated that the reduction of pH of the solution by the acid treatment significantly affected phosphate removal and implies adsorption processes accounted for 20%–40% of the total removal of phosphate. The possible

adsorption mechanism for the removal of phosphate using MCAAC could be an adsorption process through the ligand exchange between phosphate and hydroxide groups on the surface of the hydroxylated Fe and Al oxides. Phosphate adsorption through ligand-exchange reactions could be predominant when the surfaces of Fe and Al oxides were protonated, which resulted in the surfaces positively charged. This explanation could be supported by the fact that iron and aluminum oxides had higher adsorption capacity for phosphate [33]. The results and characterizations show that the calcium phosphate precipitation should be a predominate mechanism for the low-concentration phosphate removal.

3.6. Phosphate adsorption kinetics study

The prediction of batch adsorption kinetics is one of the significant aspects, which can explicate the mechanism of adsorption and its potential rate-limiting steps that include mass transport and chemical reaction processes [34]. To understand reaction pathways and the time needed to achieve the equilibrium, the kinetic data are dealt with several kinetic models including pseudo-first-order and pseudo-second-order rate models, which are the most likely models to evaluate the adsorption mechanism. The pseudo-first-order model or Lagergren first-order model is written in the following equation:

$$\lg(q_e - q_t) = \lg q_e - k_1 t \tag{4}$$

where q_t and q_e are the amount of phosphate adsorbed (mg/g) at time t and equilibrium, respectively; k_1 is the rate constant of pseudo-first-order model (min⁻¹); and t is the time (min).

Pseudo-second-order model is derived on the basis of the sorption capacity of the solid phase, described as Eq. (4):

$$\frac{t}{q_t} = \frac{1}{k_2 q_e^2} + \frac{t}{q_e} \tag{5}$$

where k_2 is the pseudo-second-order rate constant (g/mg·min).

The kinetics of phosphate removal by MCAAC is shown in Fig. 11 as a function of contact time from 5 to 120 min in acidic condition (pH = 2). Result showed that phosphate removal rate by MCAAC was quite rapid in first 30 min, and then the trend became smooth until equilibrium was attained up to 120 min.

Table 3 summarizes the kinetic parameters of phosphate adsorption on MCAAC. Plots of pseudo-first-order and pseudo-second-order are shown in Fig. 12. The correlation coefficients of the pseudo-second-order adsorption kinetic models presented higher values ($R^2 = 0.999$) than those of the pseudo-first-order one. The theoretical equilibrium adsorption capacity ($q_{e,cal} = 0.041$) in the second-order kinetics equation was closer to the equilibrium adsorption capacity ($q_{e,exp} = 0.039$) obtained from the experiment, which indicated the pseudo-second-order adsorption kinetic models was more suitable to describe this adsorption process. These results illustrated that the adsorption of phosphate on MCAAC likely occurred through chemisorption where sharing or exchange of electron takes place between phosphate and the functional

Table 2
Effect of different samples on phosphate removal

Samples	Initial pH	Final pH	Phosphate removal rate (%)
CAAC	2.00	2.05	19.16
MCAAC	2.00	2.08	39.12
Fe ₃ O ₄	2.00	2.04	71.99
MCAAC	7.02	10.26	99.21

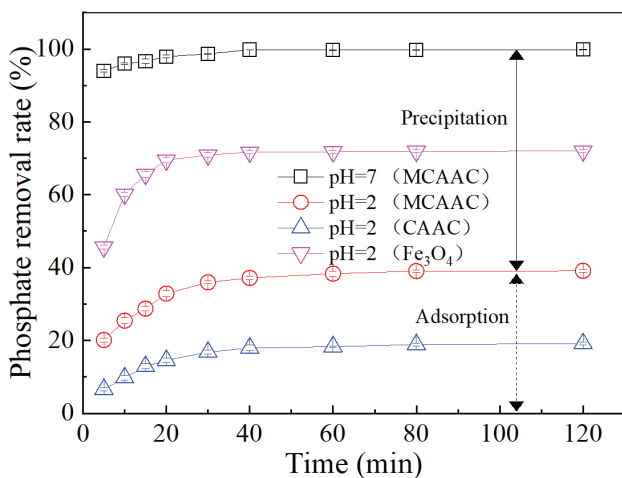


Fig. 11. Change of phosphate removal rate with MCAAC, CAAC, and Fe₃O₄ in the pH of 2 or 7 (initial phosphate concentration, 1 mg/L; contact time, 120 min; and dose of samples, 10 g/L).

Table 3

The pseudo-first-order and pseudo-second-order model adsorption constants, calculated and experimental Q_e values for phosphate removal

Sample	First-order model				Second-order model			
	$Q_{e,exp}$ (mg/g)	K_1 (min ⁻¹)	$Q_{e,cal}$ (mg/g)	R^2	$Q_{e,exp}$ (mg/g)	K_2 (min ⁻¹)	$Q_{e,cal}$ (mg/g)	R^2
MCAAC	0.039	0.031	0.029	0.968	0.039	4.675	0.041	0.999

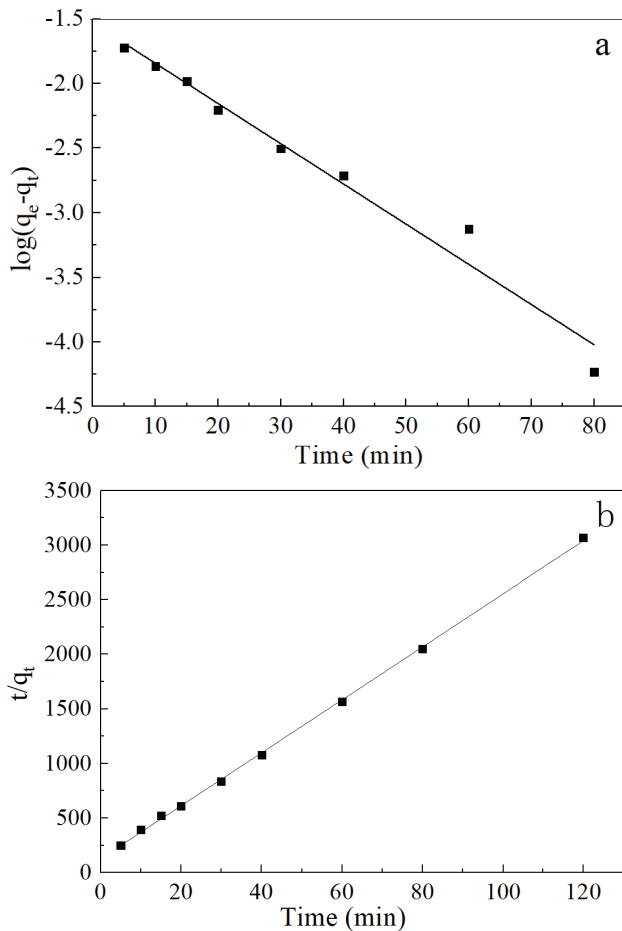


Fig. 12. Adsorption kinetics study of (a) pseudo-first order model and (b) pseudo-second order model for phosphate removal by MCAAC.

groups of MCAAC [35]. In the pseudo-second-order process, an initial surface reaction occurred until all the surface sites were occupied. Subsequently diffusion and molecular reorganization could take place at the surface for additional complexation [36].

3.7. Adsorption isotherms study

The phosphate adsorption isotherm of MCAAC in acidic condition (pH = 2) is shown in Fig. 13. The phosphate adsorption capacity considerably increased with the phosphate concentrations of applied solution increasing from 1 to 30 mg/L, which indicated that MCAAC had a certain affinity for the phosphate removal from solution. The isotherm data on phosphate adsorption were fitted to two two-parameter

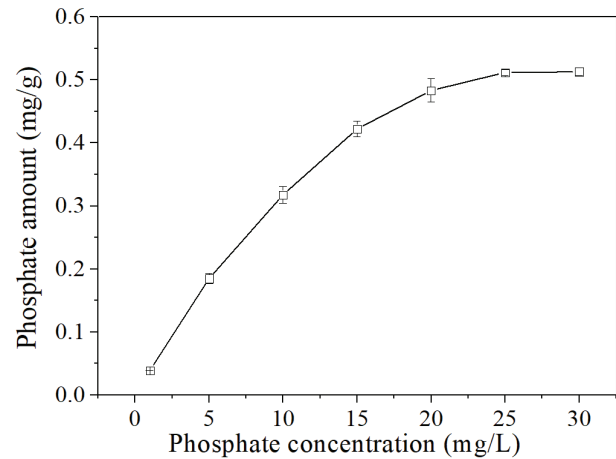


Fig. 13. Phosphate adsorption isotherm of MCAAC.

equations (Langmuir and Freundlich model). The Langmuir model assumes that a monolayer adsorption occurs on a uniform surface, which has sites of identical energy and each adsorbate molecule occupy one single site with no interaction [37]. The linear form equation of this model can be defined as follows:

$$\frac{C_e}{q_e} = \frac{1}{q_m K_L} + \frac{C_e}{q_m} \quad (6)$$

where q_e is the adsorption capacity of phosphate at equilibrium concentration (mg/g); q_m is the maximum adsorption capacity of adsorbent (mg/g); C_e represents the equilibrium concentration of the adsorbate, and K_L is the Langmuir constant which is related to the affinity of binding sites (L/mg).

The Freundlich isotherm predicts the non-ideal and reversible adsorption, which happens on an energetically heterogeneous surface, and the capacity of solute adsorbed on adsorbent enhances infinitely with increase in the concentration [38]. The logarithmic form of the Freundlich isotherm is represented by the following equation:

$$\ln q_e = \ln K_F + \frac{1}{n} \ln c_e \quad (7)$$

where K_F (mg/g); n are Freundlich constants related to the capacity and intensity of adsorption, respectively.

The fitting plots based on isotherm models for adsorption of phosphate are shown in Fig. 14. Individual adsorption parameters and the correlation coefficients were obtained by plotting the experimental data in the two different

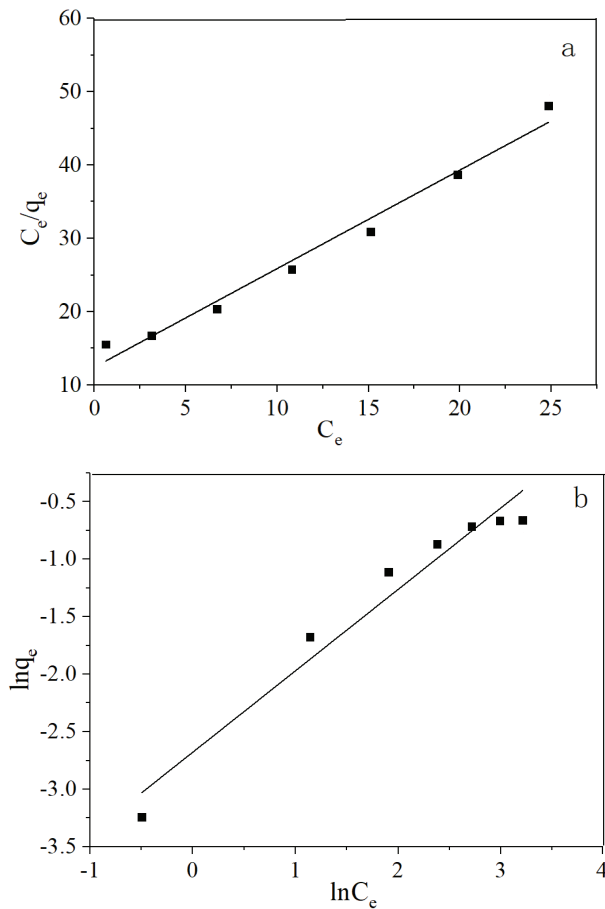


Fig. 14. (a) Langmuir and (b) Freundlich adsorption isotherms for phosphate removal by MCAAC.

Table 4

The Langmuir, Freundlich model adsorption isothermal constants, correlation coefficients, and the adsorption capacities of MCAAC for adsorption of phosphate

Sample	Langmuir			Freundlich		
	Q_m (mg/g)	K_L (L/g)	R^2	$1/n$	K_F (mg/g)	R^2
MCAAC	0.744	0.108	0.977	0.708	0.068	0.949

isotherm models, as presented in Table 4. Results showed that both Langmuir and Freundlich equations were suitable for the description of phosphate adsorption isotherm by MCAAC, but the Langmuir equation gave a better fit than the Freundlich equation according to their correlation coefficient, which meant a monolayer adsorption. The maximum adsorption capacity values measured from the Langmuir isotherm model is 0.744 mg/g for phosphate, which is close to the experimental observation.

4. Conclusion

In this work, a novel MCAAC as a carrier had been successfully synthesized and employed to separate low-concentration phosphate present in the water system.

Results showed that the phosphate removal by MCAAC was most successful at neutral pH value. Meanwhile, the factors including pH value and calcium ion concentration exerted a positive influence on phosphate removal. The mechanism for phosphate removal by MCAAC included the physical adsorption and calcium-phosphate precipitation, where the latter was more significant. According to the results of characterization, HAP ($\text{Ca}_5(\text{OH})(\text{PO}_4)_3$) was formed on the surface of MCAAC after phosphate removal. The isotherm studies elaborated that the adsorption of phosphate fitted to Langmuir model and pseudo-second-order kinetic model. Finally, the MCAAC with its excellent purification capacity and easy separation advantage could be a promising material for the removal of phosphate in low concentration from aqueous solution.

Acknowledgment

This work was supported by Major Science and Technology Program for Water Pollution Control and Treatment (2017ZX07202004, 2014ZX07206001, and 2014ZX07206005) and the Science and Technology Plan Project of Guangzhou (201510010006).

References

- [1] R.H. Li, J.J. Wang, B.Y. Zhou, M.K. Awasthi, A. Ali, Z.Q. Zhang, A.H. Lahori, A. Mahar, Recovery of phosphate from aqueous solution by magnesium oxide decorated magnetic biochar and its potential as phosphate-based fertilizer substitute, *Bioresour. Technol.*, 215 (2016) 209–214.
- [2] J.L. Stoddard, S.V. Sickle, A.T. Herlihy, J. Brahney, S. Paulsen, D.V. Peck, R. Mitchell, A.I. Pollard, Continental-scale increase in lake and stream phosphorus: are oligotrophic systems disappearing in the United States?, *Environ. Sci. Technol.*, 50 (2016) 3409–3415.
- [3] E.H. Kim, S.B. Yim, H.C. Jung, E.J. Lee, Hydroxyapatite crystallization from a highly concentrated phosphate solution using powdered converter slag as a seed material, *J. Hazard. Mater.*, 136 (2006) 690–697.
- [4] J.A. Marshall, B.J. Morton, R. Muhlack, D. Chittleborough, C.W. Kwong, Recovery of phosphate from calcium-containing aqueous solution resulting from biochar-induced calcium phosphate precipitation, *J. Cleaner Prod.*, 165 (2017) 27–35.
- [5] G. Zelmanov, R. Semiat, Phosphate removal from aqueous solution by an adsorption ultrafiltration system, *Sep. Purif. Technol.*, 132 (2014) 487–495.
- [6] Z.X. Wu, Z.M. Yu, X.X. Song, Y.Q. Yuan, X.H. Cao, Y.B. Liang, Application of an integrated methodology for eutrophication assessment: a case study in the Bohai Sea, *Chin. J. Oceanol. Limnol.*, 31 (2013) 1064–1078.
- [7] F.F. Wu, X. Wang, Eutrophication evaluation based on set pair analysis of Baiyangdian Lake, North China, *Proc. Environ. Sci.*, 13 (2012) 1030–1036.
- [8] A. Oehmen, P.C. Lemos, G. Carvalho, Z.G. Yuan, J. Keller, L.L. Blackall, M.A. Reis, Advances in enhanced biological phosphorus removal: from micro to macro scale, *Water Res.*, 41 (2007) 2271–2300.
- [9] A.H. Caravelli, C.D. Gregorio, N.E. Zaritzky, Effect of operating conditions on the chemical phosphorus removal using ferric chloride by evaluating orthophosphate precipitation and sedimentation of formed precipitates in batch and continuous systems, *Chem. Eng. J.*, 209 (2012) 469–477.
- [10] S.G. Lu, S.Q. Bai, L. Zhu, H.D. Shan, Removal mechanism of phosphate from aqueous solution by fly ash, *J. Hazard. Mater.*, 161 (2009) 95–101.
- [11] M. Kumar, M. Badruzzaman, S. Adham, J. Oppenheimer, Beneficial phosphate recovery from reverse osmosis (RO)

- concentrate of an integrated membrane system using polymeric ligand exchanger (PLE), *Water Res.*, 41 (2007) 2211–2219.
- [12] K. Ooi, A. Sonoda, Y. Makita, M. Torimura, Comparative study on phosphate adsorption by inorganic and organic adsorbents from a diluted solution, *J. Environ. Chem. Eng.*, 5 (2017) 3181–3189.
- [13] Y.J. Xue, H.B. Hou, S.J. Zhu, Characteristics and mechanisms of phosphate adsorption onto basic oxygen furnace slag, *J. Hazard. Mater.*, 162 (2009) 973–980.
- [14] X.Y. Song, Y.Q. Pan, Q.Y. Wu, Z.H. Cheng, W. Ma, Phosphate removal from aqueous solutions by adsorption using ferric sludge, *Desalination*, 280 (2011) 384–390.
- [15] K. Mandel, A.D. Tuhtan, F. Hutter, C. Gellermann, H. Steinmetz, G. Sextl, Layered double hydroxide ion exchangers on superparamagnetic microparticles for recovery of phosphate from waste water, *J. Mater. Chem. A*, 1 (2013) 1840–1848.
- [16] A.Z. Maor, R. Semiat, H. Shemer, Adsorption-desorption mechanism of phosphate by immobilized nano-sized magnetite layer: interface and bulk interactions, *J. Colloid Interface Sci.*, 363 (2011) 608–614.
- [17] A.Z. Maor, R. Semiat, H. Shemer, Synthesis, performance, and modeling of immobilized nano-sized magnetite layer for phosphate removal, *J. Colloid Interface Sci.*, 357 (2011) 440–446.
- [18] B.L. Chen, Z.M. Chen, S.F. Lv, A novel magnetic biochar efficiently sorbs organic pollutants and phosphate, *Bioresour. Technol.*, 102 (2011) 716–723.
- [19] W.J. Wang, H.P. Zhang, L. Zhang, H.Q. Wan, S.R. Zheng, Z.Y. Xu, Adsorptive removal of phosphate by magnetic $\text{Fe}_3\text{O}_4/\text{C}@\text{ZrO}_2$, *Colloids Surf. A*, 469 (2015) 100–106.
- [20] M. Rashid, N.T. Price, M.A.G. Pinilla, K.E. O’Shea, Effective removal of phosphate from aqueous solution using humic acid coated magnetite nanoparticles, *Water Res.*, 123 (2017) 353–360.
- [21] U. Berg, D. Donnert, A. Ehbrecht, W. Bumiller, I. Kusche, P.G. Weidler, R. Nüesch, “Active filtration” for the elimination and recovery of phosphorus from waste water, *Colloids Surf. A*, 265 (2005) 141–148.
- [22] W.G. Fu, P.P. Li, Characteristics of phosphorus adsorption of aerated concrete in wastewater treatment, *Adv. Mater. Res.*, 183–185 (2001) 466–470.
- [23] S. Malavipathirana, S. Wimalasiri, N. Priyantha, S. Wickramasooriya, A. Welagedara, G. Renman, Value addition to waste material supported by removal of available phosphate from simulated brackish water—a low cost approach, *J. Geosci. Environ. Prot.*, 1 (2013) 7–12.
- [24] E. Oğuz, A. Gürses, N. Canpolat, Removal of phosphate from wastewaters, *Cem. Concr. Res.*, 33 (2003) 1109–1112.
- [25] W.J. Li, L.X. Zeng, Y. Kang, Q.Y. Zhang, J.W. Luo, X.M. Guo, A solid waste, crashed autoclaved aerated concrete, as a crystalline nucleus for the removal of low concentration of phosphate, *Desal. Wat. Treat.*, 57 (2015) 14169–14177.
- [26] H. Faghihian, M. Moayed, A. Firooz, M. Irvani, Synthesis of a novel magnetic zeolite nanocomposite for removal of Cs^+ and Sr^{2+} from aqueous solution: kinetic, equilibrium, and thermodynamic studies, *J. Colloid Interface Sci.*, 393 (2013) 445–451.
- [27] H. Faghihian, M. Moayed, A. Firooz, M. Irvani, Evaluation of a new magnetic zeolite composite for removal of Cs^+ and Sr^{2+} from aqueous solutions: kinetic, equilibrium and thermodynamic studies, *C.R. Chim.*, 17 (2014) 108–117.
- [28] L.X. Zeng, M.J. Xie, Q.Y. Zhang, Y. Kang, X.M. Guo, H.J. Xiao, Y. Peng, J.W. Luo, Chitosan/organic rectorite composite for the magnetic uptake of methylene blue and methyl orange, *Carbohydr. Polym.*, 123 (2015) 89–98.
- [29] X.C. Chen, H.N. Kong, D.Y. Wu, X.Z. Wang, Y.Y. Lin, Phosphate removal and recovery through crystallization of hydroxyapatite using xonotlite as seed crystal, *J. Environ. Sci.*, 21 (2009) 575–580.
- [30] M. Hermassi, C. Valderrama, J. Dosta, J.L. Cortina, N.H. Batis, Evaluation of hydroxyapatite crystallization in a batch reactor for the valorization of alkaline phosphate concentrates from wastewater treatment plants using calcium chloride, *Chem. Eng. J.*, 267 (2015) 142–152.
- [31] Y.W. Chen, J.L. Wang, Preparation and characterization of magnetic chitosan nanoparticles and its application for Cu(II) removal, *Chem. Eng. J.*, 168 (2011) 286–292.
- [32] H.Y. Zhu, R. Jiang, L. Xiao, G.M. Zeng, Preparation, characterization, adsorption kinetics and thermodynamics of novel magnetic chitosan enwrapping nanosized $\gamma\text{-Fe}_2\text{O}_3$ and multi-walled carbon nanotubes with enhanced adsorption properties for methyl orange, *Bioresour. Technol.*, 101 (2010) 5063–5069.
- [33] J.G. Chen, H.N. Kong, D.Y. Wu, X.C. Chen, D.L. Zhang, Z.H. Sun, Phosphate immobilization from aqueous solution by fly ashes in relation to their composition, *J. Hazard. Mater.*, 139 (2007) 293–300.
- [34] J. Febrianto, A.N. Kosasih, J. Sunarso, Y.H. Ju, N. Indraswati, S. Ismadji, Equilibrium and kinetic studies in adsorption of heavy metals using biosorbent: a summary of recent studies, *J. Hazard. Mater.*, 162 (2009) 616–645.
- [35] A. Gücek, S. Şener, S. Bilgen, M.A. Mazmançı, Adsorption and kinetic studies of cationic and anionic dyes on pyrophyllite from aqueous solutions, *J. Colloid Interface Sci.*, 286 (2005) 53–60.
- [36] F.Z. Xie, F.C. Wu, G.J. Liu, Y.S. Mu, C.L. Feng, H.H. Wang, J.P. Giesy, Removal of phosphate from eutrophic lakes through adsorption by in situ formation of magnesium hydroxide from diatomite, *Environ. Sci. Technol.*, 48 (2014) 582–590.
- [37] S.S. Tahir, N. Rauf, Removal of a cationic dye from aqueous solutions by adsorption onto bentonite clay, *Chemosphere*, 63 (2006) 1842–1848.
- [38] Y.J. Yoon, W.K. Park, T.M. Hwang, D.H. Yoon, W.S. Yang, J.W. Kang, Comparative evaluation of magnetite-graphene oxide and magnetite-reduced graphene oxide composite for As(III) and As(V) removal, *J. Hazard. Mater.*, 304 (2016) 196–204.